Hindawi
Advances in Civil Engineering
Volume 2023, Article ID 9865205, 1 page
https://doi.org/10.1155/2023/9865205

*Retraction*

# Retracted: Experimental Study on Mineral Solid Waste Green Grouting Material Based on Electromagnetic Characteristic Detection

**Advances in Civil Engineering**

Received 10 October 2023; Accepted 10 October 2023; Published 11 October 2023



This article has been retracted by Hindawi following an investigation undertaken by the publisher [1]. This investigation has uncovered evidence of one or more of the following indicators of systematic manipulation of the publication process:

(1) Discrepancies in scope
(2) Discrepancies in the description of the research reported
(3) Discrepancies between the availability of data and the research described
(4) Inappropriate citations
(5) Incoherent, meaningless and/or irrelevant content included in the article
(6) Peer-review manipulation

The presence of these indicators undermines our confidence in the integrity of the article's content and we cannot, therefore, vouch for its reliability. Please note that this notice is intended solely to alert readers that the content of this article is unreliable. We have not investigated whether authors were aware of or involved in the systematic manipulation of the publication process.

Wiley and Hindawi regrets that the usual quality checks did not identify these issues before publication and have since put additional measures in place to safeguard research integrity.

We wish to credit our own Research Integrity and Research Publishing teams and anonymous and named external researchers and research integrity experts for contributing to this investigation.

The corresponding author, as the representative of all authors, has been given the opportunity to register their agreement or disagreement to this retraction. We have kept a record of any response received.

## References

[1] X. Wang, J. Hu, X. Zhang, K. Wang, D. Shen, and C. Liang, "Experimental Study on Mineral Solid Waste Green Grouting Material Based on Electromagnetic Characteristic Detection," *Advances in Civil Engineering*, vol. 2022, Article ID 6261429, 19 pages, 2022.

Hindawi
Advances in Civil Engineering
Volume 2022, Article ID 6261429, 19 pages
https://doi.org/10.1155/2022/6261429

*Research Article*

# Experimental Study on Mineral Solid Waste Green Grouting Material Based on Electromagnetic Characteristic Detection

**Xiangpeng Wang**,[1,2] **Jin Hu**,[2,3] **Xiang Zhang**,[1] **Kunpeng Wang**,[1] **Di Shen**,[1] **and Chuntao Liang**[1]

[1]*College of Geophysics, Chengdu University of Technology, Chengdu 610059, China*
[2]*Tsinghua University, Department of Civil Engineering, Sichuan Mianzhu New Building Materials Co., Ltd., High Performance Green Building Materials Joint Research and Development Center, Deyang 618200, China*
[3]*Sichuan College of Architecture Technology, Deyang 618000, China*

Correspondence should be addressed to Xiangpeng Wang; wangxiangpeng@stu.cdut.edu.cn and Jin Hu; 478428210@qq.com

Received 12 November 2021; Revised 27 December 2021; Accepted 11 January 2022; Published 18 March 2022

Academic Editor: Ramadhansyah Putra Jaya



The production processes for the gypsum- and cement-based materials, which are widely used in civil engineering projects, require the consumption of large amounts of energy and natural resources. At the present time, the main development directions of civil engineering material include realizing solid waste recycling and the applications of green building materials, which can be then used in the fields of disaster treatment and ecological restoration, such as grouting materials. In addition, the grouting quality is always difficult to detect. This study examined the gypsum- and cement-based green grouting materials made from mineral solid waste used in disaster and cloud detection by means of electromagnetic characteristics. According to the requirements of electrical testing of grouting quality, first we designed a material made with solid waste. Then, we studied the resistivity, strength, porosity, and other physical and mechanical properties of the material. The test results of the material and its soaking solution indicate that this material is a green material meeting the environmental safety standards. The experimental results show that the rapid detection of grouting quality can be realized. The following effects on electromagnetic characteristics and mechanical properties of the green materials of gypsum- and cement-based were analyzed. The results showed that the resistivity and strength were related to the ratios of the water content to the modified phosphogypsum; the percentages of cement content in the total amount of modified phosphogypsum and marble powder; the percentages of marble powder in the modified phosphogypsum; the percentages of steel fiber content in the phosphogypsum; and the fineness of the marble powder. The field test results also confirm that the green grouting material can be effectively applied in engineering repair imaging monitoring.



## 1. Introduction

The production processes for the gypsum- and cement-based materials, which are widely used in civil engineering projects, require the consumption of large amounts of energy and natural resources. At the present time, the main development directions of civil engineering material design include solid waste recycling and the applications of green building materials. A primary focus is to realize the recycling of solid waste materials, which can then be used in the fields of disaster treatment and ecological restoration.

In recent years, many countries throughout the world have made major progress in mining, metal smelting, coal power generation, and chemical production. However, at the same time, large quantities of industrial waste products have been discharged during the production processes. If industrial waste residue is not used, it will not only occupy valuable land resources but will also result in air pollution, soil pollution, and water pollution. However, it has been determined that industrial waste residue has utilization value. On the premise of meeting the requirements of environmental safety, industrial waste residue can be used as a

part of the cement- and gypsum-based materials applied to ecological restoration and disaster management projects, thereby reducing carbon emissions and improving some of the properties of civil engineering materials [1–3].

In the field of civil engineering, grouting is an important technical means for the rapid control of engineering disasters and the reinforcement of weak strata. It has been widely used in slope control, mining, and tunnel water shutoff emergencies [1–8]. At the same time, the backfill of mining goafs and reinforcement of urban underground spaces must be treated before construction can begin, in order to avoid damages to upper structures caused by uneven surface deformations. The most common treatment scheme involves grouting filling. For example, after construction is completed, the traditional detection methods include drilling, water pressure tests, surface deformation monitoring, and so on [9–11]. However, the monitoring of the construction processes cannot be effectively carried out, and only fixed-point detections can be completed for the detection points. These types of detections are not only time-consuming but also involve high cost and still may be unable to comprehensively grasp the grouting situation in a timely manner. Therefore, it can be seen that the workloads of detection and monitoring processes are large, and the original geological conditions may be seriously damaged.

To accurately understand the diffusion processes and scope of underground spaces from the aspect of slurry and visualize the relevant information, several geophysical methods can be adopted. Such combinations have the advantages of high efficiency and large-area detection results when detecting concealed work areas and can be combined with other detection methods to realize the "point surface combination" in three-dimensional detections [12]. The most commonly used geophysical detection methods include high-density electrical; transient Rayleigh waves; geological radar; transient electromagnetic; magnetotelluric; cross hole seismic wave CT; cross hole electromagnetic wave CT methods [13–17]. S. H. Adnan, R. Hamdan, and N. A. Roni introduced an alternative method, which reuses the RCA as a water filter medium to remove phosphorus from wastewater [18]. In addition, Sang L., Idowu T., and Okumu V. examined the viability of waste marble dust (WMD), an industrial waste produced during the shaping and polishing of marble blocks, as well as during its extraction from mines, as a mineral filler in hot-mix asphalt (HMA) concrete [19]. Hossain, M. B., Roknuzzaman, M., Biswas, M. A., and Islam, M., considered since there is a possibility of leaching by dumping a large quantity of fly ash in the pond, the use of fly ash from the power plants to improve soft cohesive soils for road subgrade may be an environment-friendly alternative to its disposal in the ponds [20]. Adewumi, J. R., Ajibade, T. F., and Ajibade, F. O., studied undertaken to assess the present status of on-site sanitation facilities in public places within Akure, to trace problems related to sanitation and solid waste management [21]. Kam, C. Z., and Kueh, A. B. H., discussed on the major existing methodologies in pursuing sustainable value of polymeric materials [22]. However, the previous studies had only detected the grouting treatment effects of mining goafs based on cement and fly ash materials. When compared with cement and fly ash materials, gypsum-based and cement-based composite materials have the advantages of high setting rates (close to 100%); easy transportation; easy control of the diffusion range; and no water separation during solidification. Therefore, such material can be gradually applied in goaf backfilling and other projects. In summary, at the present time, the grouting treatment effects of gypsum- and cement-based composites for mining goafs have become new research topics.

Previous studies [23, 24] have shown that when fluid flows and diffuses in the stratum, the movement of water and slurry in the rock soil spaces will transfer the electrical charges and cause changes in the geoelectric potential and currents, which are sensitive to changes in slurry diffusion. Many researchers have investigated the variations of electric fields during the process of groundwater seepage (Hamdi FAI et al., 2012; Rupesh et al., 2021) [25–27]. A large number of research studies have been carried out regarding the law of seepage, diffusion of grout, and the effects of grouting filling from the aspects of theoretical analysis, experimental research, and engineering practices both in China and internationally, and major achievements have been made [28–30]. It is generally believed that transient electromagnetic methods have the advantages of no primary field background interference; no high resistance shielding effects; no static effects; and minimal influencing effects of terrain. Such methods are also especially sensitive to low resistance. However, there have been few reports presented on whether natural electrical fields and artificial electrical fields can be used to reflect the infiltration and diffusion of slurry during the process of grouting in porous rock and soil. That is to say, slurry diffusion in geological structures [31–40].

The characteristics of the medium resistivity of cement and fly ash slurry after solidification have been thoroughly investigated. However, the changes in resistivity of gypsum-based and cement-based material slurry before and after solidification have rarely been studied. According to this study's experimental design, the correlations between the resistivity changes of different gypsum- and cement-based materials, and other properties of gypsum- and cement-based materials, were analyzed in depth. Then, based on the obtained experimental results, the feasibility of detecting the grouting effects of gypsum- and cement-based materials were deferred using electrical characteristics. In addition, tests of the application effects were performed in practical engineering scenarios. The goals of this study were to provide a new method for the detection of material grouting effects and to promote the resource utilization of solid waste in the construction of ecological environments. The research results of this study can potentially be used to detect filling conditions after grouting and to determine whether the conditions meet the physical and mechanical properties of the design requirements. The electrical differences between the grouting material and the surrounding rock, soil, or other materials can also be utilized to realize the monitoring and detection of disaster control grouting engineering processes.

## 2. Raw Materials

*2.1. Cement.* In the present investigation, 425 ordinary Portland cement was obtained from the Xi'an Yaobai cement plant. It was confirmed that its performance met the national standards (Table 1).

*2.2. Phosphogypsum.* In order to verify the different types of mineral admixtures, two different types of phosphogypsum were used in this experiment. The modified phosphogypsum used in this study was dihydrate phosphogypsum provided by Mianzhu Panlong Co. (Table 2). The modified phosphogypsum powder was hemihydrate gypsum produced by Mianzhu Co. (Table 3).

*2.3. Steel Fiber.* Hebei Zhitai Steel Fiber Manufacturing Co., Ltd., provided the steel fiber utilized in this study (Table 4).

*2.4. Basalt Fiber.* The basalt fiber was produced by Deyang Zhongxin Co. (Table 5).

*2.5. Marble Powder.* According to the details of previous related experiments, marble powder respectively milled for 1, 5, 30, and 120 minutes will exhibit different characteristics. The particle distributions and properties are shown in Figure 1 and Table 6. In this study's orthogonal experiment, these were represented by finenesses of 1, 2, 3, and 4, respectively.

*2.6. Sand.* The sand utilized in the experiments was obtained from Mianzhu Construction Investment Co. It was confirmed to meet the national requirements (Table 7). The gradation is shown in Table 8, which also met the requirements. The fineness modulus was 3.08, which was considered to be medium sand.

*2.7. Water Reducing Agent.* This study adopted a YSNF-A6 superplasticizer provided by Shanxi Yongsheng Building Materials Chemical Co., Ltd. The water reduction rate was 17%; bleeding rate was 45%; and gas content was 2.4%. The setting timeframe was 25 to 65 minutes. The compressive strength ratios were as follows: 1 d: 153%; 3 d: 143%, 7 d: 130%, and 28 d: 126%. Compressive strength ratio refers to the strength of the specimen with water reducing agent in the same age divided by the strength without water reducing agent.

*2.8. Retarder.* This study used SG-09 gypsum retarder produced by Suzhou Xingbang Chemical Building Materials Co., Ltd. The powder was white to yellowish in color. The water content was ≤3%, and the *pH* value (20% aqueous solution, 20°C) ranged between 10 and 13.

## 3. Experimental Testing Scheme

*3.1. Compressive Strength.* Some factors affecting resistivity and strength of concrete are studied, such as the ratio of cement content to the total amount of modified phosphogypsum and marble powder, and the ratio of steel fiber content to phosphogypsum. Therefore, a five-factor and four-level orthogonal test method was used in this research investigation to design the mix proportion, and the testing scheme is shown in Table 9.

In the present study, the marble powder with finenesses of 1, 2, 3, and 4, respectively, refers to marble powder D50 37.87 $\mu$m, 31.70 $\mu$m, 29.74 $\mu$m, and 20.42 $\mu$m. The compressive strength and flexural strength levels of mortar were tested by 40 * 40 * 40 mm, 70.7 * 70.7, and 100 * 100 * 100 mm molds for 3 days, 7 days, 28 days, and 3 months, respectively.

*3.2. Resistivity Test Scheme.* The resistivity changes observed from the beginning of the forming processes were tested by applying a resistance tester.

*3.3. Porosity Test Scheme.* The changes in the porosity levels were tested using a magnetic resonance instrument. A nonevaporating water content method was also tested.

*3.4. Environmental Safety Detection Scheme.* The material composition was tested using an electron scanning microscope/energy spectrometer (SEM/EDS), Fourier transform infrared spectrometer (FTIR), gas chromatography mass spectrometry (GCMS), and inductively coupled plasma emission spectrometer (ICP-OES). The test was performed according to standards GB/T6040-2019, GB/T9722-2006, GB/T17359-2012, and EPA6010D-2018. After the sample had been soaked for 24 hours, the composition of the soaking solution was tested in the same way.

## 4. Results and Analysis

*4.1. Compressive and Flexural Strength.* As shown in Figure 2, the strength levels of the 3 d, 7 d, and 28 d and 6 m (i.e., maintenance for 6 months) were observed to have increased. Group 8 had the highest strength on day 3, while Group 4 had the highest strength on days 7 and 28. The proportion of water in Group 9 was larger than that in Group 4, while the proportions of steel fiber and cement were smaller than that in Group 4. It was observed that the relationships among the early strength levels and the steel fiber content, cement content, and water cement ratios were minimal. However, the late strength level of Group 9 was observed to be lower than the others, which indicated that the previously mentioned factors had mainly affected the later strength levels. The ratio of water to solid material in Group 4 was 0.32, and that of Group 8 was 0.5, while the proportion of steel fiber in solid material was 0.12 in Group 4 and 0.083 in Group 8.

Table 1: Cement properties content and other natural requirements.

| Chemical composition | $SiO_2$ | $Fe_2O_3$ | $Al_2O_3$ | CaO | MgO | $SO_3$ | Loss |
|---|---|---|---|---|---|---|---|
| Content (%) | 22.63 | 3.83 | 5.71 | 58.95 | 1.89 | 2.62 | 4.37 |

| | Chemical composition content (%) | | | Specific surface area | Water requirement of normal consistency (%) | Setting time (min) | | Flexural strength (MPa) | | Compressive strength (MPa) | |
|---|---|---|---|---|---|---|---|---|---|---|---|
| | Loss | MgO | $SO_3$ | $m^2/kg$ | | Initial setting | Final setting | 3 d | 28 d | 3 d | 28 d |
| Index requirements | ≤5.0 | ≤5.0 | ≤3.5 | ≥300 | | ≥45 | ≤600 | ≥3.5 | ≥6.5 | ≥17.0 | ≥42.5 |
| Experimental data | 4.37 | 1.89 | 2.62 | 354 | 27.5 | 182 | 235 | 5.7 | 7.8 | 31.5 | 56.9 |
| Single evaluation | Standard | Standard | Standard | Standard | Standard | Standard | Standard | Standard | Standard | Standard | Standard |

Table 2: Modified phosphogypsum ($CaSO_4 \cdot 2H_2O$) properties.

| Inspection items | Experimental data (%) |
|---|---|
| I.oss | — |
| $SiO_2$ | — |
| $Fe_2O_3$ | — |
| $Al_2O_3$ | — |
| CaO | 31.56 |
| MgO | — |
| $SO_3$ | 42.68 |
| Water soluble fluorine | Not detected |
| Water soluble phosphorus pentoxide | 0.008 |
| $P_2O_3$ | 0.36 |
| F | Not detected |
| Attached water | — |
| Crystal water | 16.98 |
| C3A | — |

Table 3: Modified phosphogypsum powder (CaSO4·1/2H2O) properties.

| Inspection items | | Unit | Index requirements | | | Experimental data | Single evaluation |
|---|---|---|---|---|---|---|---|
| | | | 3.0 | 2.0 | 1.6 | | |
| B-CaSO4·1/2H2O | | % | | >60.0 | | 68.7 | Standard |
| Fineness (0.2 mm square hole sieve residue) | | % | | ≤10 | | 3 | Standard |
| Setting time | Initial setting time | min | | ≥3 | | 4 | Standard |
| | Final setting time | min | | ≤30 | | 8 | Standard |
| 2 h flexural strength | | Mpa | ≥3.0 | ≥2.0 | ≥1.6 | 3.4 | Standard |
| 2 h compressive strength | | Mpa | ≥6.0 | ≥4.0 | ≥3.0 | 7.0 | Standard |
| Radioactivity | IRa | — | | ≤1.0 | | — | — |
| | Ir | — | | ≤1.0 | | — | — |
| Restricting element | $K_2O$ | % | Agreed by both parties | | | 0.16 | — |
| | $Na_2O$ | % | Agreed by both parties | | | 0.11 | — |
| | MgO | % | Agreed by both parties | | | 0.96 | — |
| | $P_2O_5$ | % | Agreed by both parties | | | 1.80 | — |
| | F | % | Agreed by both parties | | | 0.10 | — |

Table 4: Steel fiber properties.

| | Diameter (mm) | Length (mm) | Aspect ratio | Tensile strength (MPa) | Bending performance, bending core 3 mm |
|---|---|---|---|---|---|
| Index requirements | 0.55 ± 0.055 | 35 ± 3.5 | 60 ± 6 | ≥1000 | Cold bend 90°, 9/10continuous |
| Experimental data | 0.55 | 35.10 | 64 | 1265 | 20/20 continuous |
| Single evaluation | Standard | Standard | Standard | Standard | Standard |

Table 5: Basalt fiber properties.

| | Diameter ($\mu$m) | Length (mm) | Breaking strength (MPa) | Elongation at break (%) | Elastic modulus (MPa) | Alkali resistance (%) | Density (g/cm$^3$) | Appearance |
|---|---|---|---|---|---|---|---|---|
| Index requirements | 9–25 | — | ≥1200 | ≤3.1 | ≥8.0 * 103 | ≥75 | 2.60–2.80 | Uniform color and no pollution |
| Experimental data | 16.5 | 18 | 1354 | 3.1 | 57.3 * 103 | 95.4 | 2.62 | Uniform color and no pollution |
| Single evaluation | Standard | — | Standard | Standard | Standard | Standard | Standard | Standard |

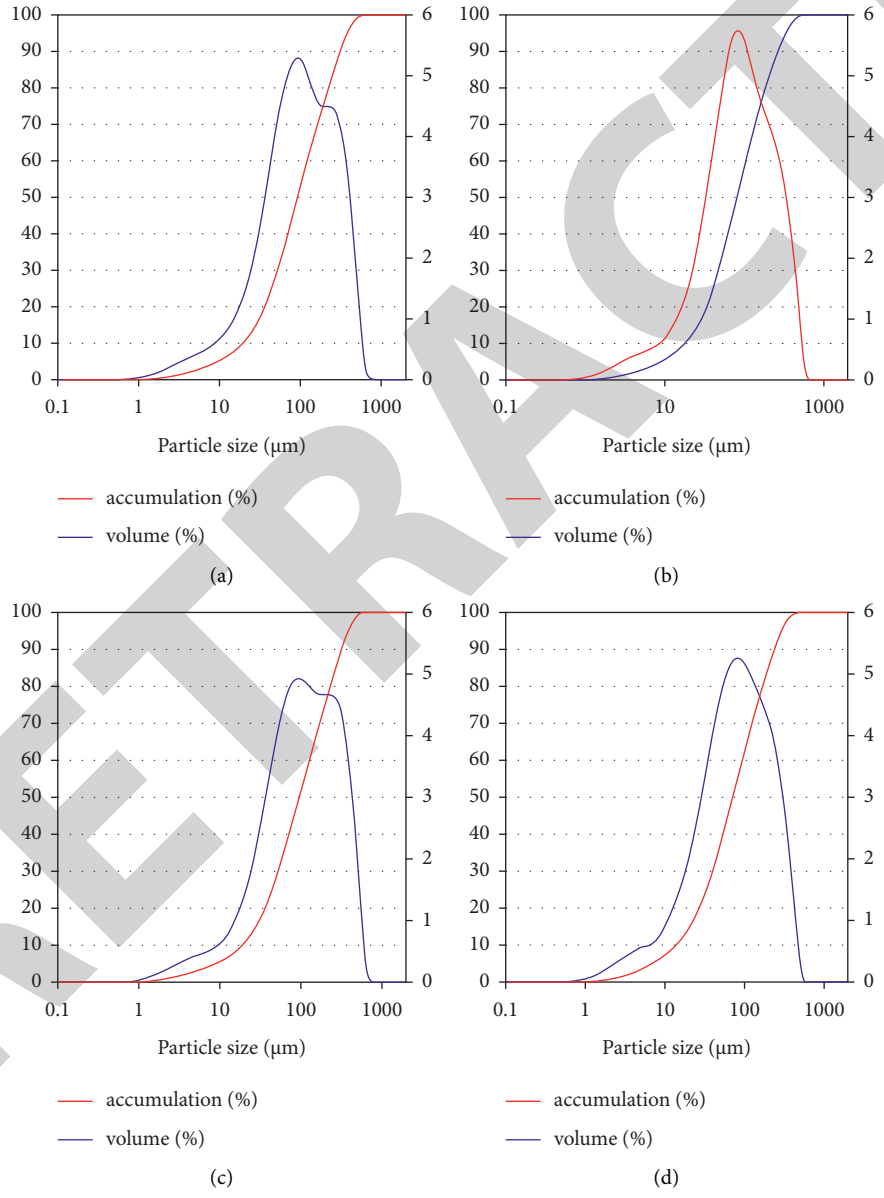


Figure 1: Particle size distributions of marble powder under different grinding time: (a) particle distribution grinding for 1 minute; (b) particle distribution grinding for 5 minutes; (c) particle distribution grinding for 30 minutes; (d) particle distribution grinding for 120 minutes.

Group 4, which had a large steel fiber proportion and small water proportion, had the highest strength in the later stage. It can be seen that the ratio of steel fiber and water was more important in the later stage, while Group 8, which had small steel fiber and large water proportion, had higher strength in the early stage. It can also be seen that the ratio of water to

Table 6: Marble powder properties.

| | CaO + MgO (%) | Color | Free water (%) | Volume stability |
|---|---|---|---|---|
| High-class index requirements | ≥70 | — | 0.4–2 | Qualified |
| Experimental data | 100 | Higher white interference co]our | 0 | Qualified |
| Single evaluation | Standard | — | Standard | Standard |

Table 7: Sand properties.

| | | | | | | | | |
|---|---|---|---|---|---|---|---|---|
| Mesh size(mm) | 4.75 | 2.36 | 1.18 | 0.6 | 0.3 | 0.15 | Sieve bottom | — |
| Cumulative percentage retained (%) | 5.99 | 23.13 | 48.27 | 73.91 | 83.54 | 90.21 | 94.27 | — |
| Apparent density (g/cm$^3$) | 2.651 | Mud content (%) | 1.0 | Clay content (%) | | | 0.1 | |
| Fineness modulus | 3.08 | Soundness (%) | 2 | Mica content (%) | | | 0.21 | |
| 0rganic matter content | | — | | SO3 content (%) | | | 0.12 | |

Table 8: Material grading table.

| Aperture (mm) | 5 | 2.5 | 1.25 | 0.625 | 0.31 | 0.16 | <0.16 |
|---|---|---|---|---|---|---|---|
| Cumulative sieve residue percentage (%) | 5.99 | 23.13 | 48.27 | 73.91 | 83.54 | 90.21 | 100 |

Table 9: Experimental scheme.

| Serial number | Ratio of water to modified phosphogypsum $A$ | Percentage of cement content in total amount of modified phosphogypsum and marble powder $B$ (%) | Percentage of marble powder in modified phosphogypsum $D$ (%) | Percentage of steel fiber content in phosphogypsum $E$ (%) | Fineness of marble powder |
|---|---|---|---|---|---|
| 1 | 0.55 | 5 | 10 | 20 | 1(1) |
| 2 | 0.55 | 15 | 0 | 10 | 3(30) |
| 3 | 0.55 | 20 | 20 | 5 | 4(120) |
| 4 | 0.55 | 25 | 40 | 40 | 2(5) |
| 5 | 0.6 | 5 | 20 | 40 | 3 |
| 6 | 0.6 | 15 | 40 | 5 | 1 |
| 7 | 0.6 | 20 | 10 | 10 | 2 |
| 8 | 0.6 | 25 | 0 | 20 | 4 |
| 9 | 0.65 | 5 | 40 | 10 | 4 |
| 10 | 0.65 | 15 | 20 | 20 | 2 |
| 11 | 0.65 | 20 | 0 | 40 | 1 |
| 12 | 0.65 | 25 | 10 | 5 | 3 |
| 13 | 0.7 | 5 | 0 | 5 | 2 |
| 14 | 0.7 | 15 | 10 | 40 | 4 |
| 15 | 0.7 | 20 | 40 | 20 | 3 |
| 16 | 0.7 | 25 | 20 | 10 | 1 |

solid materials and the proportion of steel fiber were not the most important factors affecting the strength at the late age.

As can be seen in Figure 3, the compressive strength increased with age, with Group 13 being the slowest. The fastest increase was observed in Group 4. The compressive strength of Group 13 was also low and increased slowly in the three ages. However, since the marble powder dosage was 0, it was indicated that the marble powder had not degraded the strength. The intensity of Group 4 increased rapidly, so that it became much higher than the other groups other than Group 3, and it was the highest after 28 d. The special proportion of the fourth group is the use of 6% naphthalene water reducer. It can be seen from the SEM photograph shown in Section 4.2 that the crystal structure and density of Group 4 with water reducing agent are completely different from those without water reducing agent. It is speculated that this is the result of its chemical reaction, and further research is in progress.

The strength measured after soaking for 3 d in proportioning 4 is only 0.401 MPa, but it reaches 8.7907 Mpa after 28 d and 8.8075 Mpa after soaking for 7 d. The strength of standard curing is also 0.6521 and 1.1612 MPa after 3 and 7 d, respectively, while it reaches 14.5133 MPa after 28 d. The strength in the later stage is greatly improved. It is quite different from the intensity growth mode of other groups. In addition, at 6 months, the compressive strengths of Groups 1 and 6 were lower than at 28 d.

As mentioned in Figure 4, the flexural strength had not increased with age, and the flexural strength levels of Groups

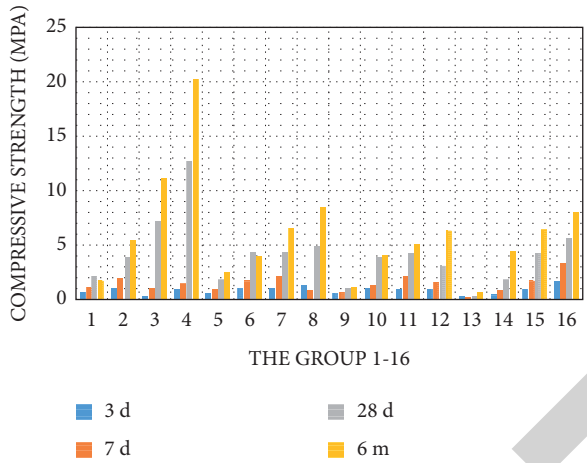


Figure 2: 3 d, 7 d, 28 d, and 6-month compressive strength.

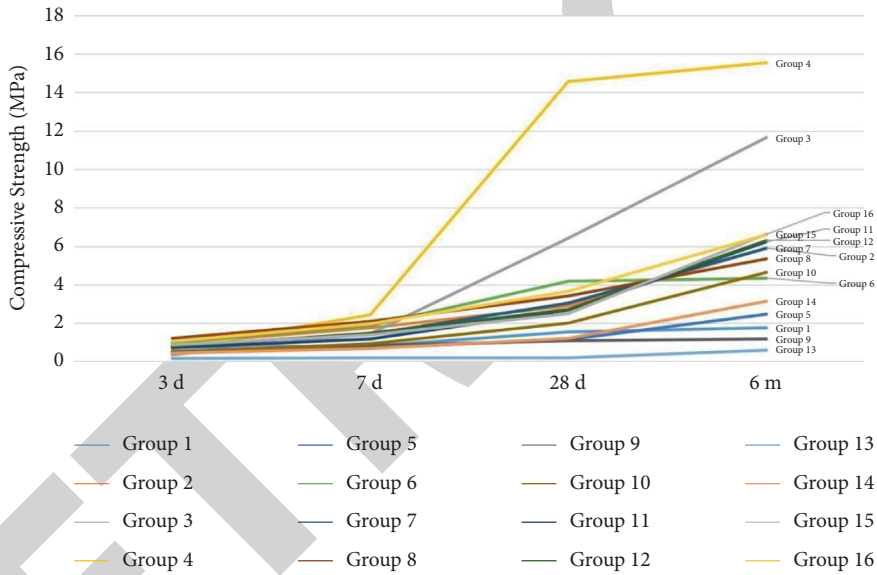


Figure 3: Variation trends of the compressive strength levels.

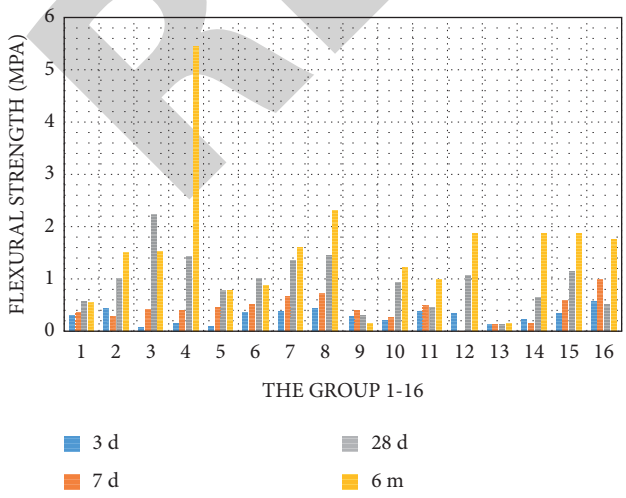


Figure 4: 3 d, 7 d, 28 d, and 6-month flexural strength.

9, 11, 13, and 16 decreased on day 28. In particular, the strength levels of Group 9 and Group 13 were the lowest at 28 d, which was similar to the compressive strength. Groups 1, 3, 6, and 9 had intensities of less than 28 d after 6 months. The 28 d resistivities of Groups 1, 6, 9, and 13 are higher, which shows that there is some connection among them, and the reason behind this is being further studied.

As can be seen in Figure 5, the change trends of the compressive strength and flexural strength were not the same. The flexural strengths at 3 d and 7 d were the highest in Group 16, and the flexural strength at 6 months was the highest in Group 4. The compressive strength at 3 d was the highest in Group 8, and the flexural strengths at 7 d and 6 months were the highest in Group 4. The compressive strength increases from 3 d to 6 months, while the flexural strengths of Groups 1, 6, and 9 of three months were even lower than that of 7 d. Therefore, the underlying mechanism requires further studied.

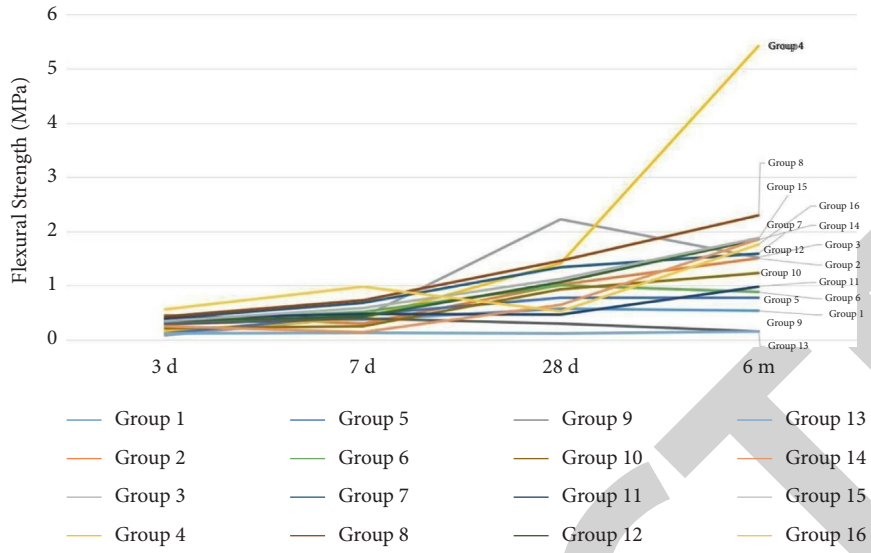


Figure 5: Change trends of the flexural strength levels.

*4.2. Micromorphology.* The reason for which SEM images are selected for comparison is that the later flexural strengths of Groups 1, 6, and 9 are lower than those in the early age, while the strength of Group 4 is very high, and the strength increases significantly compared with that in the early age.

The microscopic imagery of Group 4's observations showed that the crystal was much more highly dense than the other groups, and the crystal shape was clear (Figure 6–11). Its high strength is also likely related to this.

The strength of ratio 3 is only second to 4, while the crystal density of ratio 3 is also second only to 4.

*4.3. Element Content.* According to the element content shown in Table 10, the highest strength of ratios 3 and 4 is likely due to the absence of P. P is the element phosphorus, which has a retarding effect on concrete, and its enrichment easily causes the eutrophication of environmental water. The reason for the lowest strength of ratio 13 is likely the highest content of S.

*4.4. Resistivity Changes.* The testing data are detailed in Figure 12. We can see that the sample with high resistivity in three days has high resistivity in seven days. This characteristic can help us to quickly detect the properties of materials.

As shown in Figure 13, the change trends of the resistivity were not consistent with the that of the compressive strength. However, there were some similarities observed with the change rules of the flexural strength.

*4.5. Porosity Changes.* When the results shown in Figure 14 were compared with those shown in Figure 12, it can be seen that the variation trends of the porosity were contrary with those of the resistivity. In addition, as shown in Figure 13, the change trends of the porosity were basically the same during all the different ages. Also, the change trends of the strength during the different ages were basically the same, and the smaller the resistance was, the greater the porosity would be. The change trend of nonevaporated water content is shown in Figure 15. It can be seen that it is highly consistent with the change trend of resistivity shown in Figure 12, thus indicating that the nonevaporated water content is directly related to resistivity.

*4.6. Environmental Safety Detection Results.* The component test results of the material and its soaking solution are shown in Tables 11 and 12. No substances affecting environmental safety appear in the soaking solution, indicating that this material is a green material, which meets environmental safety standards.

## 5. Analysis of the Data

*5.1. Analysis of the Influencing Factors of the Optimal Strength.* According to the calculation and analysis rules of the orthogonal experiment, the following results are determined based on the table. Due to the large size of the table and space constraints, combined with the fact that the data are reflected in the previous figure, the process is omitted from the table.

It can be seen from Tables 13 and 14 that the main and secondary influencing factors of the compressive strength were the proportions of cement content in the total amount of modified phosphogypsum and marble powder; fineness of the marble powder; proportions of steel fiber content in the phosphogypsum; proportions of water and modified phosphogypsum; and proportions of marble powder in the modified phosphogypsum.

*5.2. Analysis of the Influencing Factors of the Resistivity Optimization.* As detailed in Tables 15 and 16, the primary and secondary influencing factors of the resistivity were the percentages of steel fiber content in the phosphogypsum.

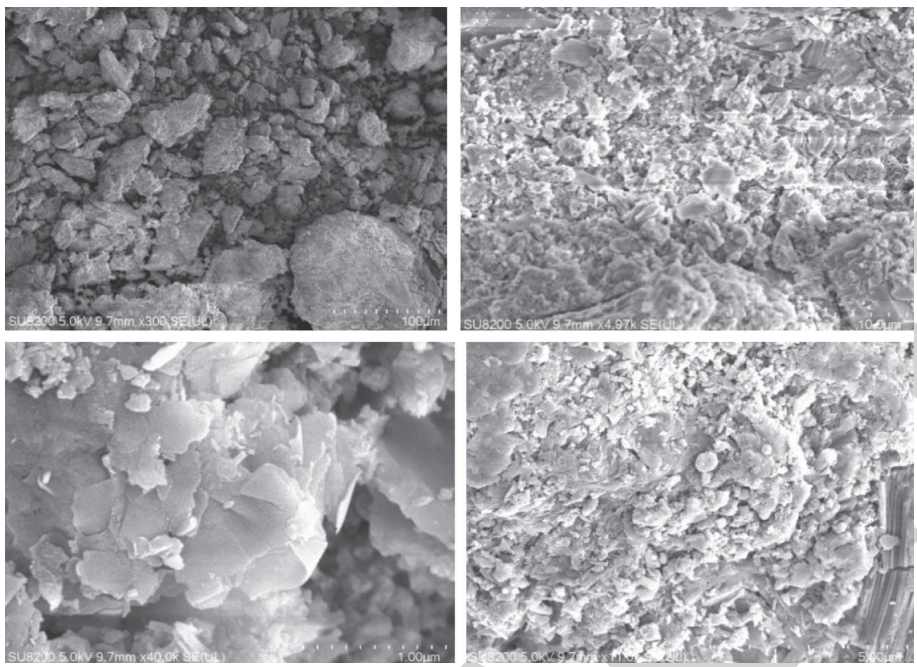

Figure 6: Microstructure of Group 4.

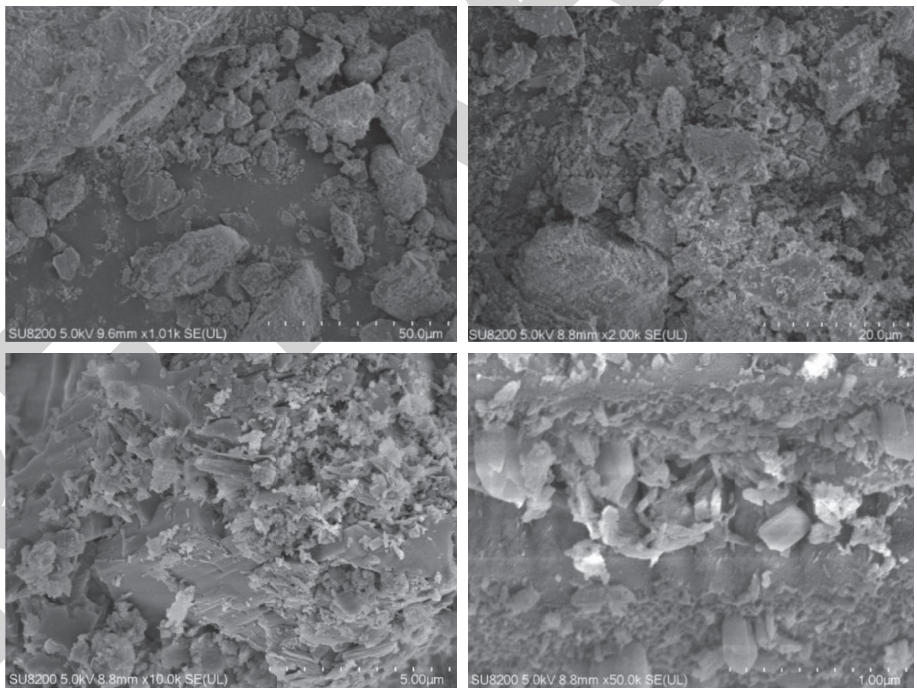

Figure 7: Microstructure of Group 1.

This was followed by the proportions of water and modified phosphogypsum; percentage of marble powder in the modified phosphogypsum; fineness of the marble powder; and the percentage of cement content in the total amount of modified phosphogypsum and marble powder.

*5.3. Parallel Tests and Analysis of the Optimal Strength Ratios.* The parallel experiment mentioned here refers to that performed under the condition of the same amount of other materials, except for the fact that the amount of marble powder is changed to compare the influence of the change of

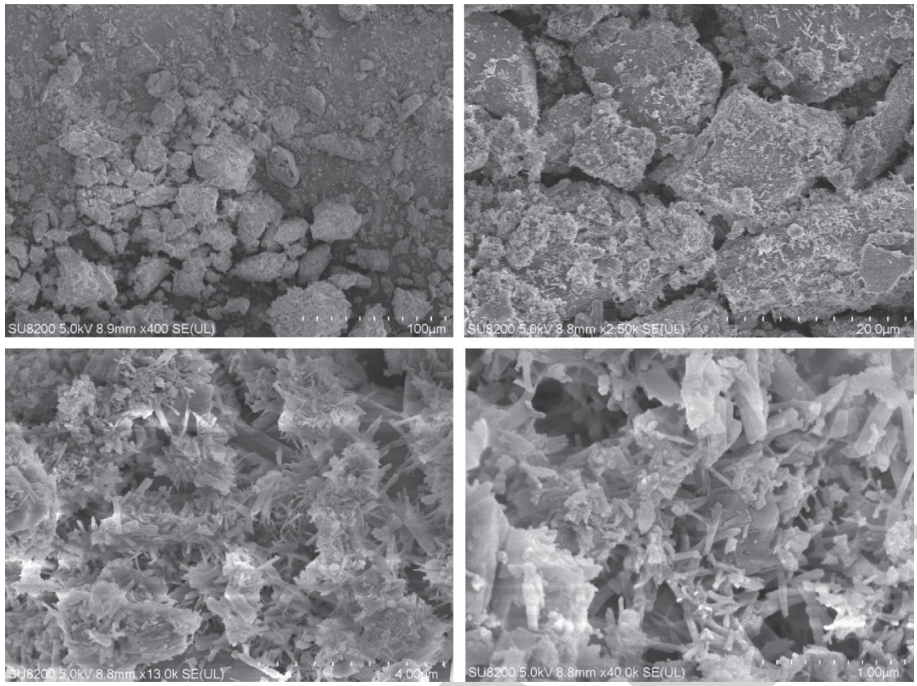


Figure 8: Microstructure of Group 6.

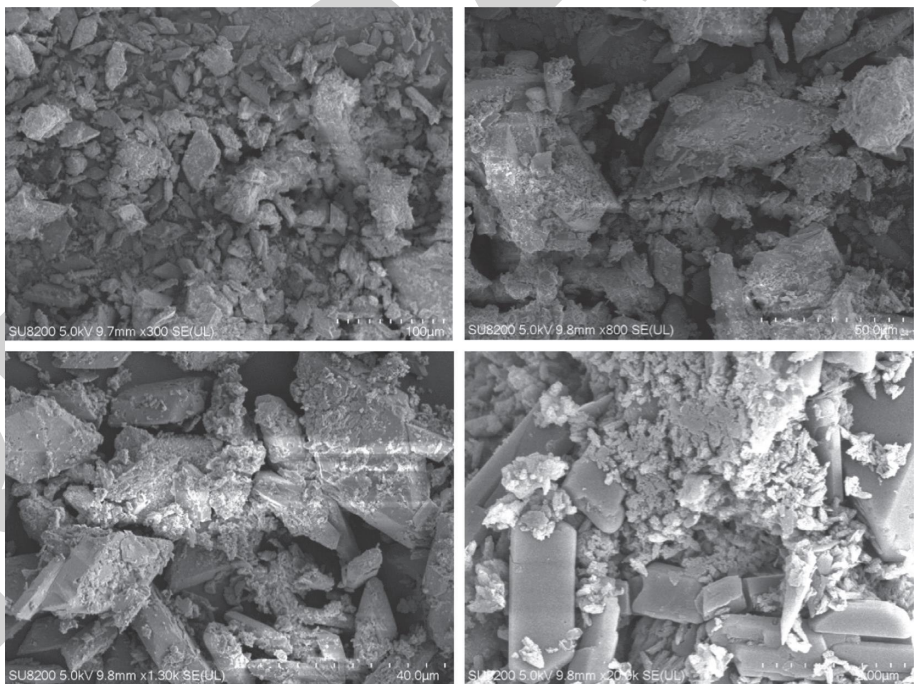


Figure 9: Microstructure of Group 13.

single conditions, which is different from the above orthogonal experiment.

In this study, in accordance with the identified influencing factors and the analysis of the optimal ratios, the parallel test ratio of the optimal ratio was obtained, as shown in Table 17.

The strength test results of the optimal ratio are shown in Table 18.

It was determined that the most effective dosage of marble powder for the 3 d strength was 100. For the 7 d compressive strength, the most effective marble powder content was 50, while the flexural strength was the best when

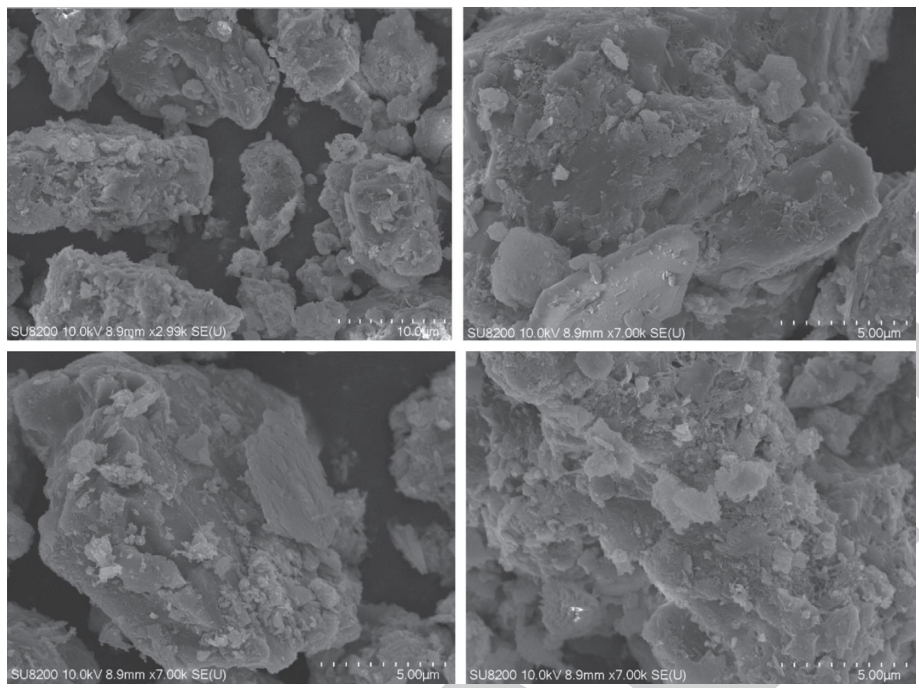


Figure 10: Microstructure of Group 3.

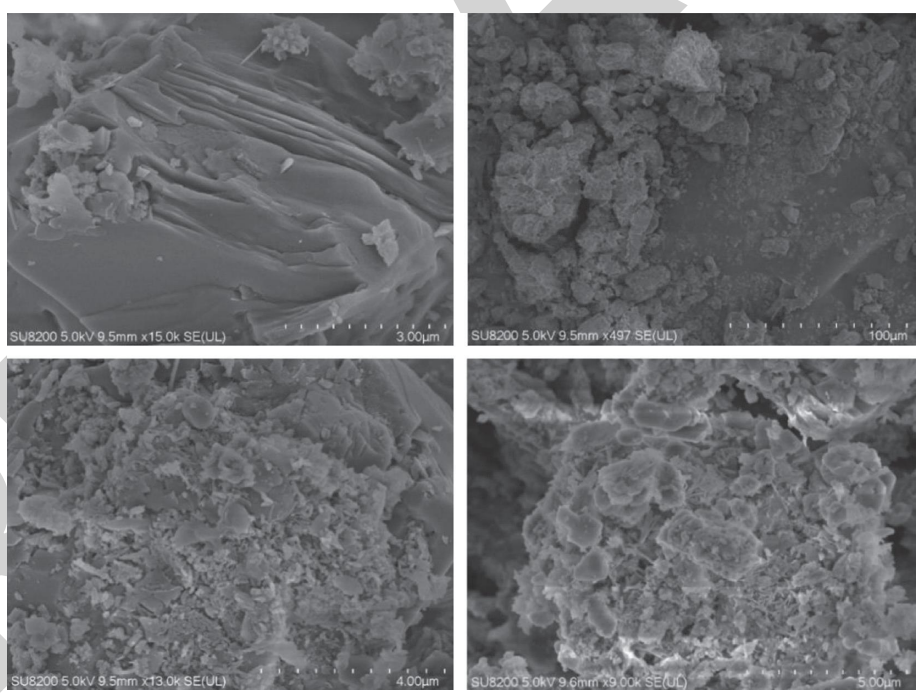


Figure 11: Microstructure of Group 9.

Table 10: Element content.

| Element content(%) | C | O | Na | Mg | Al | Si | P | S | K | Ca | Fe | Au |
|---|---|---|---|---|---|---|---|---|---|---|---|---|
| Group 1 | 21.82 | 51.87 | | | 1.63 | 3.08 | 0.79 | 5.24 | 0.24 | 6.52 | | 8.81 |
| Group 3 | 43.05 | 32.97 | 0.12 | 0.1 | 0.69 | 1.51 | | 4.9 | 0.11 | 12.08 | 0.36 | 4.11 |
| Group 6 | | 49.47 | | 0.71 | 1.82 | 7.39 | 0.46 | 6.32 | 0.7 | 21.48 | 1.29 | 10.35 |
| Group 9 | 6.04 | 24.95 | 0.31 | 0.25 | 1.72 | 3.41 | 0.93 | 9.74 | 0.42 | 41.97 | 1.6 | 8.67 |
| Group 13 | | 46.91 | 0.31 | 0.28 | 1.72 | 6.06 | 0.83 | 14.27 | 0.26 | 20.41 | 1.72 | 7.24 |
| Group4 | | 49.81 | | 0.57 | 1.21 | 3.59 | | 10.87 | 0.32 | 28.33 | 1.74 | 3.56 |

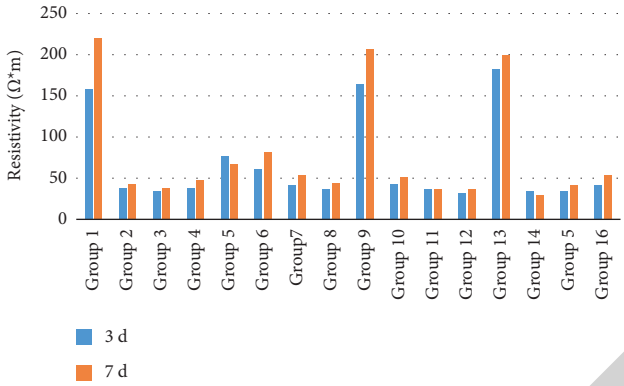


Figure 12: Resistivity.

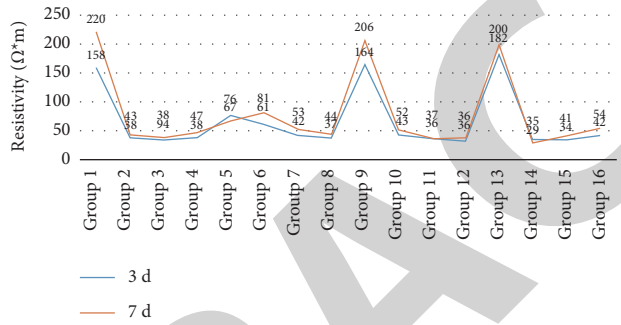


Figure 13: Change trends of the resistivity.

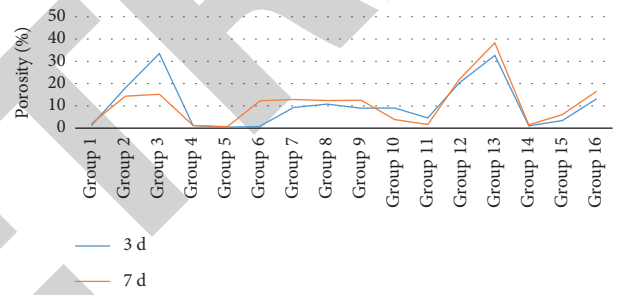


Figure 14: Change trends of the porosity.

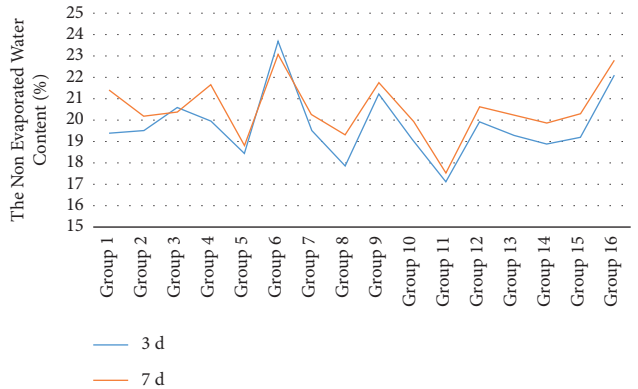


Figure 15: Change trends of the nonevaporated water content.

Table 11: Material composition.

| Component | Content (%) |
|---|---|
| $CaCO_3$ | 46.3 |
| $CaSO_4$ | 29.8 |
| $Al_2O_3$ | 3.4 |
| $Fe_2O_3$ | 1.1 |
| $MgCO_3$ | 3.9 |
| Phosphate | 0.6 |
| $TiO_2$ | 0.1 |
| $SiO_2$ | 11.8 |
| Water | 3.0 |

Table 12: Soaking solution composition.

| Component | Content(ppm) |
|---|---|
| Al | 5 |
| Ca | 603 |
| K | 9 |
| Na | 19 |
| SO42- | 1222 |

Table 13: Statistical table of the influencing factors of the 3 d strength levels.

| | Ratio of water to modified phosphogypsum powder *A* | Percentage of cement content in total amount of modified phosphogypsum and marble powder *B* (%) | Percentage of marble powder in modified phosphogypsum powder *C* (%) | Percentage of steel fiber content in phosphogypsum powder *D* (%) | Fineness of marble powder E |
|---|---|---|---|---|---|
| Primary and secondary order | | | $B > E > D > A >$ C | | |
| Optimal level | *A*2 | *B*4 | *C*1 | *D*2 | |
| Optimal combination | | | *A*2 *B*4 *C*1 *D*2*E*1 | | |

Table 14: Statistical table of the influencing factors of the 7 d strength levels.

| | Ratio of water to modified phosphogypsum powder A | Percentage of cement content in total amount of modified phosphogypsum and marble powder B (%) | Percentage of marble powder in modified phosphogypsum powder C (%) | Percentage of steel fiber content in phosphogypsum powder *D* (%) | Fineness of marble powder E |
|---|---|---|---|---|---|
| Primary and secondary order | | | $B > E > D > A >$ C | | |
| Optimal level | *A*2 | *B*4 | *C*1 | *D*2 | |
| Optimal combination | | | *A*2 *B*4 *C*1 *D*2*E*1 | | |

Table 15: Statistical table of the influencing factors of the 3 d electrical characteristics.

| | Ratio of water to modified phosphogypsum powder *A* | Percentage of cement content in total amount of modified phosphogypsum and marble powder *B* (%) | Percentage of marble powder in modified phosphogypsum powder *C* (%) | Percentage of steel fiber content in phosphogypsum powder *D* (%) | Fineness of marble powder E |
|---|---|---|---|---|---|
| Primary and secondary order | | | $D > A > C > E >$ B | | |
| Optimal level | *A*4 | *B*1 | *C*4 | *D*1 | |
| Optimal combination | | | *A*4 *B*1 *C*4 *D*1*E*2 | | |

Table 16: Statistical table of the influencing factors of the 7 d electrical characteristics.

| | Ratio of water to modified phosphogypsum powder $A$ | Percentage of cement content in total amount of modified phosphogypsum and marble powder $B$ (%) | Percentage of marble powder in modified phosphogypsum powder $C$ (%) | Percentage of steel fiber content in phosphogypsum powder $D$ (%) | Fineness of marble powder E |
|---|---|---|---|---|---|
| Primary and secondary order | $D > A > C > E > B$ | | | | |
| Optimal level | $A1$ | $B1$ | $C4$ | $D3$ | |
| Optimal combination | $A1\ B1\ C4\ D3E1$ | | | | |

Table 17: Parallel tests of the optimum ratios affecting the compressive strength levels.

| | Water(W) | Cement (C) | Modified phosphogypsum (MPG) | Modified phosphogypsum powder(MPCG) | Marble powder (WMP) | Steel fiber (SF) | Sand (S) |
|---|---|---|---|---|---|---|---|
| ZA1 | 2700 | 1060 | 2250 | 2025 | 0 | 210 | 10350 |
| ZA2 | 2700 | 1060 | 2250 | 2025 | 50 | 210 | 10350 |
| ZA3 | 2700 | 1060 | 2250 | 2025 | 100 | 210 | 10350 |
| ZA4 | 2700 | 1060 | 2250 | 2025 | 200 | 210 | 10350 |

Table 18: Strength level results of the parallel tests.

| | ZA1 | ZA2 | ZA3 | ZA4 |
|---|---|---|---|---|
| 3-day compressive strength | 1.102 | 1.0988 | 1.3173 | 1.2175 |
| 7-day compressive strength | 1.5058 | 1.9373 | 1.6037 | 1.915 |

Table 19: Resistivity test results (Ω·m).

| | ZA1 | ZA2 | ZA3 | ZA4 |
|---|---|---|---|---|
| 3d/r | 32 | 23 | 38 | 30 |
| 7d/r | 47 | 58 | 57 | 46 |

the marble powder content was 200. Resistivity tests were carried out for each ratio of the parallel tests, and the results are shown in Table 19.

Figure 16(a) shows the compressive strength of the sample and Figure 16(b) shows the resistivity of the same sample. The data change trend of Figure a and Figure b was completely similar. At the same time, according to the test results, the strength levels were high when the resistivity was high (Figures 16(a) and 16(b)). Therefore, the qualitative situation of the strength could be obtained by directly measuring the resistance, and the construction quality could be controlled for rapid detections.

## 6. Field Tests

The reason for testing the mechanical properties, environmental safety properties, and resistivity properties of the above material is to develop a material with environmental safety, mechanical requirements, and easy-to-use resistivity properties for on-site detection and monitoring. Section VI of this paper aims to apply this developed material for on-site detection, and the results show that this material can detect the grouting effect quickly and effectively through resistivity, thereby meeting our expected requirements.

The resistivity acquisition instrument used in this study's testing processes was a WDZJ-4 high-density electrical instrument produced by the Chongqing Geological Instrument Factory. In addition, RES2DINV software was utilized for the data processing and inversion imaging, and a least square method was used for the inversion. Due to the fact that the measurements of landslides are affected by terrain, terrain inversion was adopted in the inversion process. Then, the data were calculated according to formulas (1)–(3). In order to meet the depth of the slip section, the distance between the on-site measurement points was set as 10 m. Since the terrain of this study's soft soil reinforcement experiment was flat, a topographic survey was not carried out during inversion imaging, and the distance between the on-site measurement points was 1 m, as shown in Figures 17 and 18. We conducted field tests using proportions ZA2 and ZA3.

The expression of potential difference was calculated as follows:

$$U_M^{AB} = \frac{I\rho}{2\pi}\left(\frac{1}{AM} - \frac{1}{BM}\right) \tag{1}$$

$$\Delta U_{MN} = U_M^{AB} - U_N^{AB} = \frac{I\rho}{2\pi}\left(\frac{1}{AM} - \frac{1}{BM} - \frac{1}{AN} + \frac{1}{BN}\right) \tag{2}$$

The calculation formula of resistivity was performed as follows:

$$\rho = K\frac{\Delta U_{MN}}{I} \tag{3}$$

*6.1. Field Test No. 1.* The test results of the landslide after the disaster treatment point are shown in Figure 19. As can be seen in the figure, the landslide was caused by the tensile fracturing of the red bed rock trailing edge as a result of continuous rainfall. In accordance with the previously mentioned testing results, grouting materials were prepared,

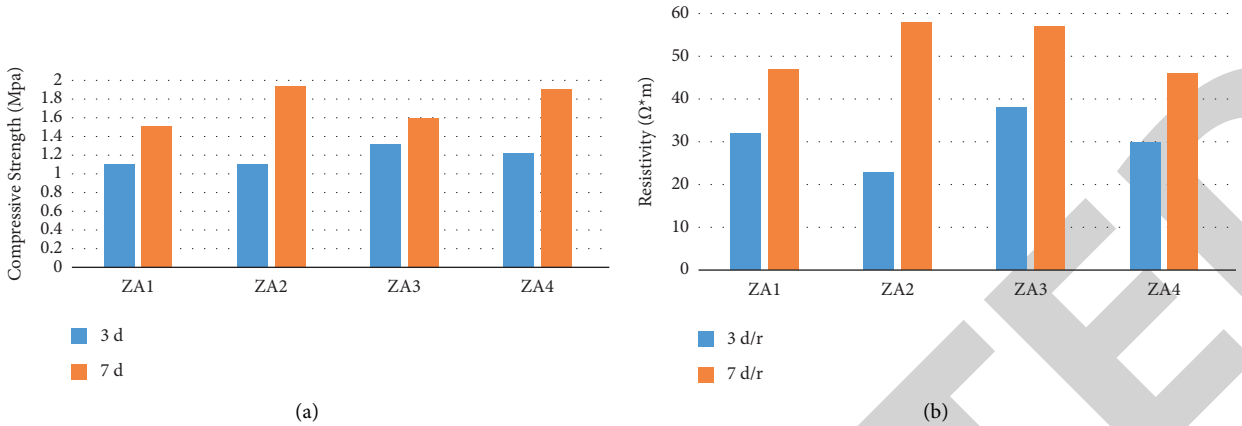


Figure 16: Comparison of strength level results.

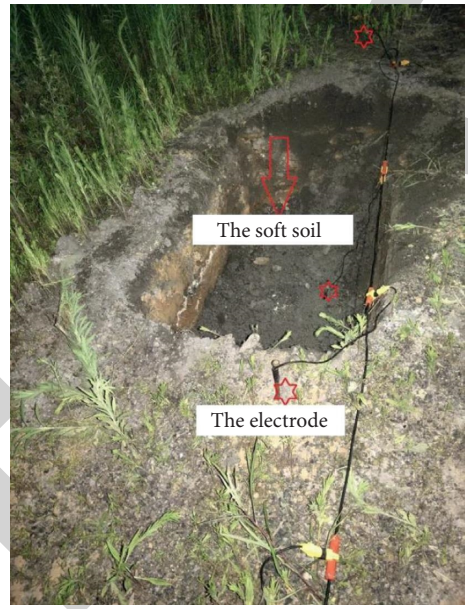


Figure 17: Experimental site images.

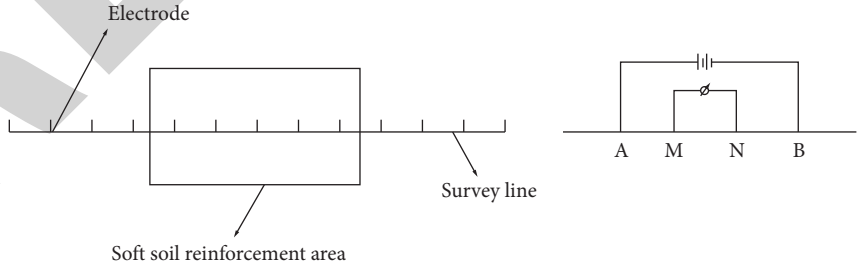


Figure 18: Schematic diagram of the experimental site.

and the strength design met the requirements of the engineering reinforcements. In addition, the electrical characteristics were taken as the detection factors of reinforcement effects. Prior to the grouting process, the rear edge of the slope body was filled with water due to rainfall and the development of cracks, which exhibited the characteristics of anomaly low resistance (indicated position before grouting). High resistance mortar was prepared according to the previously mentioned experiments and was tested three days after grouting. The original low resistance abnormal area showed high resistance anomaly (indicated position after grouting), and the resistivity of the surrounding rock was

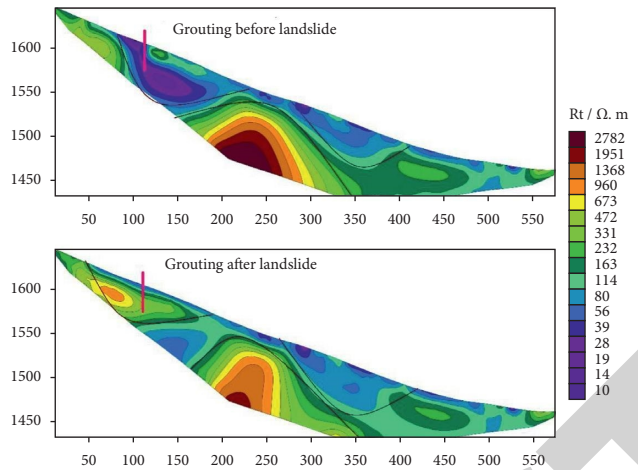


Figure 19: Experimental results of the grouting reinforcement treatment of a landslide area.

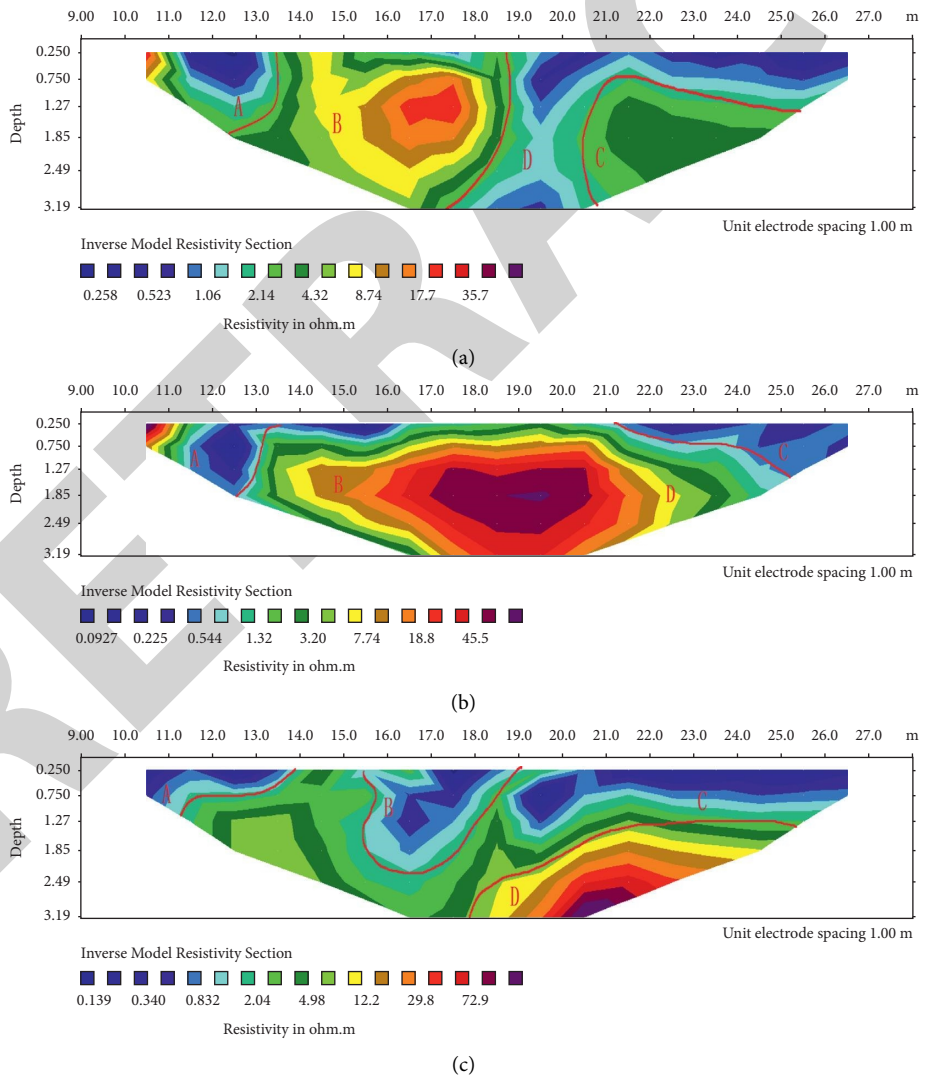


Figure 20: Soft soil reinforcement experiment: (a) electrical structure information of undisturbed stratum, (b) electrical structure information when half of the mortar is filled, and (c) formation electrical structure information after filling.

significantly increased. Therefore, the results indicated that the mortar also penetrated into the surrounding rock by filling the cracks, a good overall reinforcement of the landslide site had been formed. In summary, this field test confirmed that it was feasible to use materials with electromagnetic characteristics as the quality inspection and detection for grouting engineering.

*6.2. Field Test No. 2.* This study used the ZA2 ratios to prepare grouting material for the second field test. It can be seen in Figure 20(a) that ZA2 is selected, as its strength is moderate and quite representative. The resistivity of the undisturbed formation was abnormal and the structure was stable. The high resistivity anomaly at Point B was inferred to be an accumulation layer of landfill macroporous slag soil. Points *D* and C were determined to be the relatively low resistivity anomalies since the soil stratum had been affected by rainfall. Figure 20(b) shows the measurement results during the process of pouring grouting material ZA2 underground. Affected by manual excavation, Points C and *D* showed high resistance anomalies and symmetrical distributions, which indicated that the measurement results during the filling process were affected not only by the differences between the electrical properties of the grouting materials and surrounding rock but also by the surface shallow excavation process. Figure 20(c) shows that the measurement results after the slurry was fully filled. As can be seen in the figure, the original high resistance anomaly at Point B had disappeared, indicating that the injected slurry was basically filled. A small area of a high resistivity anomaly can be seen in the lower right corner, which may have been due to large fractures or high resistivity bodies in that area.

Through field experiments, it can be seen that the grouting materials based on mineral admixtures can be effectively applied to the ecological environment fields, such as geological disaster prevention and soft soil reinforcement. By altering the ratio of grouting materials and measuring the change of resistivity, the dynamic monitoring of grouting process and the evaluation of grouting effect can be realized.

## 7. Conclusions and Further Research Ideas

According to the previously mentioned test results, the following conclusions were drawn. (1) The resistivity was determined to be related to the proportions of water to modified phosphogypsum; percentages of cement content in the total amount of modified phosphogypsum and marble powder; percentages of marble powder in the modified phosphogypsum; percentages of steel fiber content in the phosphogypsum; and the fineness of the marble powder. Among these, the proportions of steel fiber content in the phosphogypsum were determined to be the most important factor. This was followed by the proportions of water to modified phosphogypsum; proportions of marble powder in the modified phosphogypsum; fineness of the marble powder; and the proportions of cement content in the total amount of modified phosphogypsum and marble powder. (2) According to this study's test results, the influencing factors of the resistivity and strength levels were not the same. However, the changing trend of strength and resistivity of the 3 d and 7 d samples were found to be consistent and could be used for early monitoring and detection of grouting material construction effects. (3) The component test results of the material and its soaking solution indicate that this material is a green material, which meets environmental safety standards. (4) The field test results show that the materials studied in the experiment can be used as grouting materials, and the proportion of materials can be adjusted according to the geological environmental conditions to achieve the dynamic monitoring of the grouting process and the evaluation of the effect. In the future, we will further verify the monitoring and detection advantages of grouting materials based on electromagnetic characteristics in the fields of disaster control and ecological restoration. Therefore, it was considered that the results obtained in this investigation will provide an important basis for further theoretical research and production practices.

## Data Availability

The data used to support the findings of this study are included within the article.

## Conflicts of Interest

The authors declare that they have no conflicts of interest.

## Acknowledgments

Thanks are due to Suzhou Niumag Analytical Instrument Corporation's help in NMR Experiment and analysis. This project was supported by Key R & D project of Sichuan Science and Technology plan under grant nos. 2020YFS0472 and 2019ZYZF0065.

## References

[1] H. Jin, "Late-age properties of concrete with different binders cured under 45°C at early ages," *Advances in Materials Science and Engineering*, vol. 2017, Article ID 8425718, 13 pages, 2017.

[2] H. Jin, "Comparison between the effects of superfine steel slag and superfine phosphorus slag on the long-term performances and durability of concrete," *Journal of Thermal Analysis and Calorimetry*, vol. 128, no. 10, pp. 1251–1263, 2017.

[3] H. Jin, Y. Yulei, R. Xiaojiang, Y. Kui, and L. Changkun, "Application progress of phosphorus slag in green concrete," *Commercial concrete*, vol. 5, no. 3, pp. 79–81, 2015.

[4] R. Alaie, R. Jamshidi Chenari, and M. Karimpour-Fard, "Shaking table study on sand-EPS beads-mixtures using a laminar box," *Geosynthetics International*, vol. 28, no. 3, pp. 224–237, 2021.

[5] J. G. Zornberg and G. H. Roodi, "Use of geosynthetics to mitigate problems associated with expansive clay subgrades," *Geosynthetics International*, vol. 28, no. 3, pp. 279–302, 2021.

[6] J. Zhang, Z. Yang, Q. Yang, G. Yang, G. Li, and J. Liu, "Liquefaction behavior of fiber-reinforced sand based on cyclic triaxial tests," *Geosynthetics International*, vol. 28, no. 3, pp. 316–326, 2021.

[7] S. H. Liu, J. Liao, and K. W. Fan, "Repeated loading of soilbag-reinforced road subgrade," *Geosynthetics International*, vol. 28, no. 2, pp. 113–124, 2021.

[8] H. J. Kim, T. W. Park, P. R. Dinoy, and H. S. Kim, "Performance and design of modified geotextile tubes during filling and consolidation," *Geosynthetics International*, vol. 28, no. 2, pp. 125–143, 2021.

[9] C. Lv, C. Zhu, C.-S. Tang, Q. Cheng, L.-Y. Yin, and B. Shi, "Effect of fiber reinforcement on the mechanical behavior of bio-cemented sand," *Geosynthetics International*, vol. 28, no. 2, pp. 195–205, 2021.

[10] L. Zhe, W. Yan-Qing, and Z. Jian-Shan, "Mathematical model of high pressure injection cement liquid and its application," *Rock and Soil Mechanics*, vol. 26, no. 12, pp. 1972–1976, 2005.

[11] H. Hong-Yuan and R. Yao, "Analysis of driving water permeation grouting of saturated sand seam," *Rock and Soil Mechanics*, vol. 30, no. 7, pp. 2016–2020, 2009.

[12] Y. Ping, T. Yi-Qun, P. Zhen-Bin, and A. Chen, "Study on grouting simulating experiment in sandy gravels," *Chinese Journal of Geotechnical Engineering*, vol. 28, no. 12, pp. 2134–2138, 2006.

[13] S. Hui, W. Zai-Quan, and W. Jing-Jie, "Test study on seepage permeability of limestone grouting wall system," *Chinese Journal of Underground Space and Engineering*, vol. 5, no. 5, pp. 956–959, 2009.

[14] Z. Gai-Ling, Z. Kai-Yu, and S. Wang-Hua, "Experimental investigation of the impact of flow velocity on grout propagation during chemical grouting into a fracture with flowing water," *Journal of China Coal Society*, vol. 36, no. 3, pp. 403–406, 2011.

[15] M.-Q. Zhang, W.-Q. Zhang, and G.-Q. S, "Evaluation technique of grouting effect and its application to engineering," *Chinese Journal of Rock Mechanics and Engineering*, vol. 25, no. S2, pp. 3109–3118, 2006.

[16] Z. Ping-Song, W. Jian-Sheng, and L. Sheng-Dong, "Prospecting possibility with high density resistivity for quality of concrete behind segment in tunnel," *Chinese Journal of Underground Space and Engineering*, vol. 4, no. 2, pp. 331–335, 2008.

[17] P. Hu, G.-R. Zhu, and Q.-R. Wang, "Application of high density electrical resistivity method in the monitoring survey of high pressure jet-grouting project," *Geological Journal of China Universities*, vol. 16, no. 3, pp. 375–382, 2010.

[18] S. H. Adnan, R. Hamdan, and N. A. Roni, "Removal of phosphorus from synthetic wastewater using recycled concrete aggregates as a filter medium," *Journal of civil engineering, science and technology*, vol. 9, no. 1, pp. 13–26, 2018.

[19] L. Sang, T. Idowu, and V. Okumu, "Evaluation of the performance of waste marble dust as a mineral filler in hot-mix asphalt concrete," *Journal of Civil Engineering, Science and Technology*, vol. 12, no. 1, pp. 1–14, 2021.

[20] M. B. Hossain, M. Roknuzzaman, M. A. Biswas, and M. Islam, "Evaluation of engineering properties of thermal power plant waste for subgrade treatment," *Journal of Civil Engineering, Science and Technology*, vol. 12, no. 2, pp. 112–123, 2021.

[21] J. R. Adewumi, T. F. Ajibade, and F. O. Ajibade, "Appraisal of on-site sanitation facilities and solid waste management in public places within akure municipality, Nigeria," *Journal of Civil Engineering, Science and Technology*, vol. 11, no. 1, pp. 8–21, 2020.

[22] C. Z. Kam and A. B. H. Kueh, "Towards sustainable polymeric materials: zero waste, green and self-healing," *Jurnal Teknologi*, vol. 74, no. 4, 2015.

[23] H. Xin, *Study on Grouting Effect Detection of Goaf under Subgrade of New Dongdu-Pingyi Railway*, Southwest Jiaotong University, Chengdu, China, 2013.

[24] C. Zilong, *Model Test Study on Detecting Grouting Effect of Karst Subgrade by High Density Electrical Method*, Southwest Jiaotong University, Chengdu, China, 2014.

[25] Z. Xuan, *Study on Grouting Treatment Effect of Comprehensive Geophysical Detection Method in Goaf of Nanqin Line*, Southwest Jiaotong University, Chengdu, China, 2014.

[26] L. Xueliang, L. Shuzhi, and H. Jinbo, "Application of EH-4 conductivity imaging system in detection of grouting effects in goaf area," *Safety In Coal Mines*, vol. 43, no. 11, pp. 139–142, 2012.

[27] F. A. I. Hamdi and G. Morelli, "Application of cross-hole resistivity tomography in the detection of underground cavities and weak zones," in *Proceedings of the Near Surface Geoscience 2012–18th European Meeting of Environmental and Engineering Geophysics*, Paris, France, September 2012.

[28] T. P. Rupesh and S. P. Sharma, "High-resolution quasi-3D electric resistivity tomography for deciphering groundwater potential zones in lateritic terrain," *Natural Resources Research*, vol. 30, pp. 3339–3353, 2021.

[29] D. Yu, F. Guangming, and W. Chengzhen, "Experimental research on basic properties of superhigh-water packing material," *Journal of China Coal Society*, vol. 36, no. 7, pp. 1087–1092, 2011.

[30] F. Guangming, J. Kaijun, and S. Baobao, "Application and prospect of super-high-water packing material in mining engineering," *Coal Science and Technology*, vol. 43, no. 1, pp. 5–9, 2015.

[31] G.-B. Zhang, J.-L. Liu, and M. Aubert, "Interpretation of self-potential anomalies in hydrogeological exploration of volcanic areas," *Earth Science - Journal of China University of Geosciences*, vol. 21, no. 3, pp. 109–116, 1996.

[32] S.-C. Liu, X.-M. Liu, Z.-H. Jiang, T. Xing, and M. Chen, "Research on electrical prediction for evaluating water conducting fracture zones in coal seam floor," *Chinese Journal of Rock Mechanics and Engineering*, vol. 28, no. 2, pp. 348–356, 2009.

[33] L. Sheng-Dong, W. Bo, Z. Guan-Qun, S. Yang, and M. Chen, "Experimental research on mine floor water hazard early warning based on response of geoelectric field in groundwater seepage," *Chinese Journal of Rock Mechanics and Engineering*, vol. 28, no. 2, pp. 267–272, 2009.

[34] Z. Can-Tang, "The technique to detect the leakage of dam by applying the spontaneous electric field," *Progress in Geophysics*, vol. 20, no. 3, pp. 854–858, 2005.

[35] H. Zhe, W. Jieqiang, and L. Bin, "Theoretical study of osmotic grou-ting in rock mass," *Chinese Journal of Rock Mechanics and EngiNeering*, vol. 20, no. 4, pp. 492–496, 2001.

[36] L. Zhe, W. Yanqing, and Z. Jianshan, "Mathematical model of high pressure injection cement liquid and its application," *Rock and Soil Mechanics*, vol. 26, no. 12, pp. 1972–1976, 2005.

[37] Z. Minqing, Z. Wenqiang, and S. Guoqing, "Evaluation technique of grouting effect and its application to engineering," *Chinese Journal of Rock Mechanics and Engineering*, vol. 25, no. S2, pp. 3109–3118, 2006.

[38] H. Peng, Z. Guorong, and W. Qirui, "Application of high density electrical resistivity method in the monitoring survey of high pressure jet-grouting project," *Geological Journal of China UniVersities*, vol. 16, no. 3, pp. 375–382, 2010.
[39] X. Haijun, *Study on Detection Technology of Transient Electromagnetic Method in Coal Mine Ponding Goaf*, China University of Geosciences, Beijing, China, 2009.
[40] L. Jiangang, *Feasibility Analysis of Transient Electromagnetic Survey of Coal Field Goaf*, Central South University, Changsha, China, 2009.